Available online at www.sciencedirect.com
ScienceDirect
International Journal of Impact Engineering 35 (2008) 304–318
INTERNATIONAL JOURNAL OF IMPACT ENGINEERING
www.elsevier.com/locate/ijimpeng

Ballistic impact of a KEVLAR® helmet: Experiment and simulations

C.Y. Tham[a,*], V.B.C. Tan[b], H.P. Lee[a,b]

[a]*Computational Mechanics Division, Institute of High Performance Computing, 1 Science Park Road, #01-01 The Capricorn, Singapore Science Park II, Singapore 117528, Singapore*

[b]*Department of Mechanical Engineering, National University of Singapore, 9 Engineering Drive 1, Singapore 117576, Singapore*

Received 16 September 2006; received in revised form 25 September 2006; accepted 24 March 2007
Available online 20 April 2007

Abstract

This paper presents the results from experiments and AUTODYN-3D® simulations on the ballistic impact of a KEVLAR® helmet. In the experiment, spherical projectile (~11.9 g), launched from a light gas gun, strikes the helmet with an impact velocity of 205 m/s. The interaction of the projectile with the KEVLAR® helmet is captured using high-speed photography. This helmet-projectile interaction is compared with that obtained from the AUTODYN-3D® simulation. Post-test damage photos from the experiments are also compared with those from the simulations. The response of the helmet from the simulations is consistent with those from the experiments. Also included in this paper are AUTODYN-3D® simulations on two ballistics test standards for KEVLAR® helmets. They are namely the NIJ-STD-0106.01 Type II and the V_{50} requirement of the US military specification for Personal Armor System Ground Troops (PASGT) Helmet, MIL-H-44099A. For the simulation on MIL-H-44099A, a fragment-simulating projectile (FSP) strikes the helmet with an impact velocity of 610 m/s. The simulation revealed that an impact velocity above 610 m/s is required to perforate the KEVLAR® helmet. For the simulation on NIJ-STD-0106.01 Type II helmet, the projectile is a 9 mm full-jacketed bullet with a striking velocity of 358 m/s. Results from the simulation show that the KEVLAR® helmet is able to defeat a 9 mm full-jacketed bullet traveling at 358 m/s.

Keywords: KEVLAR® helmet; Ballistic impact; Bullet/ projectile; Hydrocode simulations

1. Introduction

Helmet designs have evolved over the last three millennia and the use of helmet may be as old as warfare itself. In 600 B.C. the Greeks in Sparta crafted single-piece helmet from bronze, which provided complete head protection, leaving only narrow slits in front for vision and for ventilation. Later in 250 B.C. the Romans developed several helmet designs, which included the round legionary's helmet and the gladiator's helmet, with broad brim and pierced visor, providing exceptional head, face and neck protection. The use of helmets in battle fields continued until the end of 13th century, which signaled a radical change in the emphasis on head protection. With the invention of gunpowder and the growing effectiveness of firearms over swords and spears, helmets gradually vanished from the battle scenes. The metal helmet that once protected against sword and arrows offers little protection against musket rounds. The United States Civil War provides an excellent illustration—in war soldiers donned cloth hats and caps, with little or no emphasis on head protection.

In World War I, the helmet was reintroduced because it protected the head against metal-fragments of exploding artillery shells and indirect fire. The French, owing to General Adrian, were the first to adopt the helmet as standard equipment in early 1915 [1]. The British, the Germans, and then the rest of Europe soon followed. In World War I, the German helmet provided the best protection for soldiers. It was manufactured in at least two sizes, and different head contours were accommodated by an adjustable leather lining, which provided comfort and allowed for ventilation. The typical helmet used during that period was a hardened steel shell with an inner liner and weighed about 0.5–1.8 kg. Since then, helmets have been issued to troops in all military conflicts, marking

*Corresponding author. Tel.: +65 6419 1235; fax: +65 6419 1280.
E-mail address: thamcy@ihpc.a-star.edu.sg (C.Y. Tham).

0734-743X/$ - see front matter © 2007 Elsevier Ltd. All rights reserved.
doi:10.1016/j.ijimpeng.2007.03.008

the beginning of the development of modern military helmet.

One of the longest serving helmet designs was perhaps the M1-Helmet which consists of a steel shell and an inner liner. The M1-Helmet, for nearly 30 years, had been the primary infantry helmet to American troops during World War II, Korean War and also the war in Vietnam. Although the design of the helmet provides ballistic protection against 15 g 0.45-caliber bullets with a striking velocity of 244 m/s, soldiers were not wearing it and sustaining needless brain wounds from small fragments. Some of the shortcomings of the M1-Helmet were that it retained heat and lacked comfort and fit. The fit of the M1-Helmet was perhaps the biggest drawback, and was due to the fact that the M1-Helmet came in only one size [2,3]. Other shortcomings also included weight, lack of protection in the temporal area, poor balance and inability to use communications equipment with the helmet in place. For these reasons, the New Helmet Design Program was initiated in 1972. The initiation of the program marked an important milestone in modern military helmet, and consequently the development of the PASGT (Personnel Armor System Ground Troops) Helmet.

The design of the PASGT Helmet, which bore a strong resemblance to the World War II German helmet, was able to address the shortcomings of the M1-Helmet. The PASGT Helmet comes in five sizes to accommodate the head size distribution of US Army personnel. The bulge ear sections of the helmet directly flared to the frontal opening to provide the necessary space for the use of communications equipment. The PASGT Helmet had an optimal standoff distance of 1.23 cm, allowing optimal ventilation and heat transfer and also transient deformation due to ballistic impacts. An easily adjustable cradle suspension system was incorporated into the PASGT Helmet to compensate for minor size and shape differences while maintaining the optimal standoff distance and providing a stable helmet–head interface. The PASGT Helmet was made of KEVLAR®, a trade name for DuPont's organic fiber in the aromatic polyamide (aramid) family, due to its ballistic properties. KEVLAR®, which was commercialized by DuPont in 1972, has a unique combination of high strength, high modulus, toughness and thermal stability [4]. From the KEVLAR® family of fibers, the KEVLAR® 29 Type II fabric, woven from 1500 denier fibers in a 2×2 basket weave, was used in the molding of the PASGT Helmet. Having the combination of both shape and material, the PASGT Helmet improved coverage of the head by 11% over the M1-Helmet. Overall the PASGT Helmet provides significantly more protection to the head, especially to the low frontal area, side, and occiput, than the M1-Helmet. In the fall of 1983 during its first combat action, the new PASGT Helmet was credited with saving the lives of at least two American soldiers in the invasion of Grenada. In both cases the soldiers were wearing PASGT Helmets manufactured by Gentex Corporation. Through the years, the PASGT Helmet has received widespread troop acceptance, and tentative data from the Gulf War indicated that it is able to reduce the incidence of brain wounds. Out of 24 soldiers who sustained head wounds, only three wounds involved the brain and all were from projectiles that entered from area below the helmet.

The head and neck of a soldier represent only 12% of the body area but receive up to 25% of all "hits" during combat [1]. To ensure that the PASGT Helmet is able to provide adequate protection, manufacturers subject the helmet to a series of ballistic tests. The ballistic test standards manufacturers used are (1) NIJ-STD-0106.01 Type II and (2) V_{50} requirement of the US military specification for PASGT Helmet, MIL-H-44099A. The NIJ-STD-0106.01 is a standard developed by the Law Enforcement Standards Laboratory of the National Bureau of Standards to establish performance requirements and methods of test for helmets intended to protect against gunfire. The standards classified ballistic helmets into three types by the level of performance. For Type II, higher velocity 9 mm, the ballistic helmet protects against 9 mm full metal jacket (FMJ) bullet, with nominal mass of 8.0 g and velocity of 358 ± 15 m/s. As for MIL-H-44099A, the military specification required that the V_{50} ballistic limit for a PASGT Helmet has to be at least 610 m/s (i.e. 2000 ft/s) for a 1.1 g 0.22 caliber type 2 fragment simulating projectile (FSP).

In this paper, the objectives are twofold. The first objective is to conduct a ballistic impact test to determine the response of a KEVLAR® helmet to ballistic impact. This response of the helmet from the ballistic impact test will be used as a benchmark for later comparison with that obtained from hydrocode simulation. In the impact test, a 11.9 g spherical projectile launched from a light gas gun will strike the back of the helmet with an impact velocity of 205 m/s. The interaction of the projectile with the KEVLAR® helmet will be captured using high-speed photography. The high-speed images will reveal the response of helmet during impact. Post-test damage photos of the KEVLAR® helmet will also be taken to determine the extent of the damage on the helmet. As for the hydrocode simulation, it is performed using AUTODYN-3D® v6.1.00, a commercial hydrocode. A recently implemented composite material model, AMMHIS, in that hydrocode will be used to model the response of the KEVLAR® helmet. The second objective will extend this simulation work to include the assessment of the ballistic resistance of the KEVLAR® helmet based on NIJ-STD-0106.01 Type II, higher velocity 9 mm and MIL-H-44099A, using AUTODYN-3D® simulations. In the simulation on MIL-H-44099A, a 1.1 g FSP will strike the top of the helmet with an impact velocity of 610 m/s. While in the simulation which employs the NIJ-STD-0106.01 Type II, higher velocity 9 mm as the ballistic test standard, the projectile is a 9 mm FMJ with a striking velocity of 358 m/s. Both simulations will determine whether the KEVLAR® helmet is able to defeat the FSP and the 9 mm full-jacketed bullet.

2. Experiment

In the last decade the Defense Research Establishment (DRDC), Valcartier has conducted experiments to study the transient deformations of new composite helmets and also evaluated the performance of novel helmets [5,6]. The new composite materials tested were vinyl ester resin/Spectra® fiber 900. While the novel helmets that were evaluated were produced using net-shape spraying and plasma spraying. The helmets were made of Ti-6Al-4 V and some of these Ti-6Al-4 V helmets were coated with ceramic aluminum oxide deposited by plasma spraying. The projectiles in their experiments were launched from a smooth bore gas gun.

The ballistic test presented in this paper was performed in the Impact Mechanics Laboratory at the National University of Singapore. A light gas gun with a 15 mm bore was used to accelerate the 14.9 mm diameter stainless steel spherical projectile to 205 m/s. The projectile velocity was measured based on a time-of-flight system in which the projectile's time of arrival was noted (i.e. a bleak in a continuous light signal) at two points located a known distance apart. Fig. 1 shows the setup of the experimental apparatus, which include two laser photodetectors for the time-of-flight system located near the exit of the gun barrel. The interaction of the projectile with KEVLAR® helmet was photographed by means of a FASTCAM—Ultima APX high-speed CMOS camera. The camera was operating at 50 000 frames per second. The camera was installed at an angle to the impact. The helmet in the experiment is molded from KEVLAR® 29/polyvinyl butyral-phenolic composite with 15–18% resin content. The KEVLAR® 29 fabric in the helmet is of Type II. High-speed images of the ballistic impact are shown in Fig. 2. The 11.9 g steel projectile did not penetrate the helmet. Shortly after the impact and transient deformation, debris from the paintwork on the helmet is ejected from the impact region and the projectile is seen traveling in the opposite direction.

3. Material modeling

The ballistic resistance of the KEVLAR® helmet is assessed using hydrocode simulations. The simulations are carried out using AUTODYN-3D®, a commercial hydrocode developed by Century Dynamics. A hydrocode is a computer program that is capable of computing strains, stresses, velocities and propagation of shock waves

Fig. 1. The set-up for the ballistic impact test of a KEVLAR® helmet.

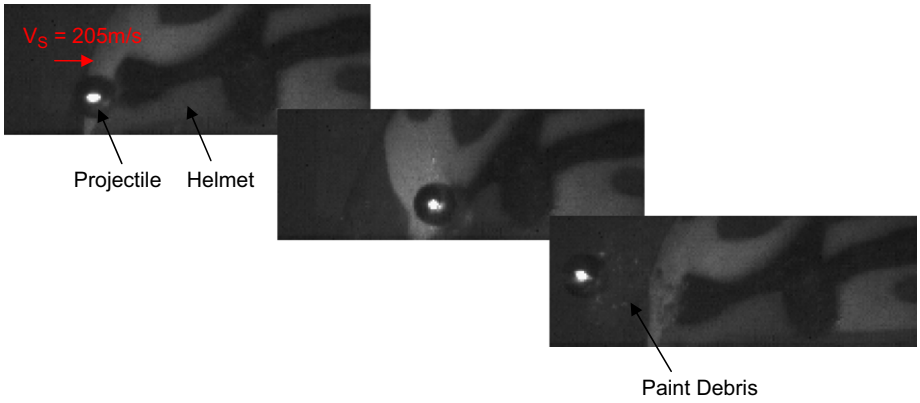

Fig. 2. High-speed images of the ballistic impact of a spherical steel projectile (~11.9 g) on a KEVLAR® helmet.

as a function of space and time. In the last two decades, hydrocodes have been used extensively to simulate the penetration and perforation of isotropic materials (i.e. steel and aluminum) subjected to high velocity impact. However, with the development of lighter and stronger fiber material (i.e. KEVLAR®, Spectra® and Zylon®) there is a growing interest in the use of hydrocode to simulate ballistic impact of anisotropic materials for the development of composite armor. Unlike isotropic materials such as steel or aluminum, the ballistic response of anisotropic materials is more complex and requires extensive material characterization. In a project with European Space Agency (ESA), Hayhurst et al. [7–9] implemented a composite material model based on an approach by Anderson and coworkers [10] in AUTODYN-2D/3D [11] that could couple anisotropic constitutive behavior with a non-linear (shock) equation of state (EOS). The composite material model in AUTODYN-2D/3D takes into account the following complex phenomena relating to the high velocity impact of anisotropic materials:

— Anisotropic strength degradation.
— Material anisotropy.
— Melting, vaporization and decomposition.
— Shock response.
— Coupling of volumetric and deviatoric response.

For completeness, the following section will describe the features of this composite material model.

3.1. Orthotropic EOS

The material model, also known as AMMHIS (advanced material model for hypervelocity impact simulation) [10], is able to calculate (1) the contributions to pressure from the isotropic and deviatoric strain components, and (2) the contributions to the deviatoric stress from the deviatoric strains. For a linearly elastic orthotropic material, the total stress, σ_{ij}, can be related to the total strain, ε_{ij}, through the orthotropic stiffness matrix, C_{ij}. The coefficients of C_{ij} are functions of the orthotropic elastic material constants, E_{ii}, v_{ij} and G_{ij}.

$$\begin{bmatrix}\sigma_{11}\\ \sigma_{22}\\ \sigma_{33}\\ \sigma_{23}\\ \sigma_{31}\\ \sigma_{12}\end{bmatrix} = \begin{bmatrix} C_{11} & C_{12} & C_{13} & 0 & 0 & 0\\ C_{21} & C_{22} & C_{23} & 0 & 0 & 0\\ C_{31} & C_{32} & C_{33} & 0 & 0 & 0\\ 0 & 0 & 0 & C_{44} & 0 & 0\\ 0 & 0 & 0 & 0 & C_{55} & 0\\ 0 & 0 & 0 & 0 & 0 & C_{66}\end{bmatrix} \begin{bmatrix}\varepsilon_{11}\\ \varepsilon_{22}\\ \varepsilon_{33}\\ \varepsilon_{23}\\ \varepsilon_{31}\\ \varepsilon_{12}\end{bmatrix}. \tag{1}$$

To separate thermodynamic (EOS) response from the ability of the material to carry shear loads (strength), it is convenient to separate the strains into their volumetric and deviatoric components. Thus the strain components are split into their average, ε_{ave}, and deviatoric, ε^{d}_{ij}, components:

$$\varepsilon_{ij} = \varepsilon^{d}_{ij} + \varepsilon_{ave}. \tag{2}$$

Now defining the average direct strain increment, ε_{ave}, as a third of the trace of the strain tensor,

$$\varepsilon_{ave} = \tfrac{1}{3}(\varepsilon_{11} + \varepsilon_{22} + \varepsilon_{33}) \tag{3}$$

and assuming, for small strain increments, the volumetric strain increment is defined as

$$\varepsilon_{vol} \approx \varepsilon_{11} + \varepsilon_{22} + \varepsilon_{33}. \tag{4}$$

The total strain increments can be expressed in terms of the volumetric and deviatoric strain increments resulting in the following orthotropic constitutive relation:

$$\begin{bmatrix}\sigma_{11}\\ \sigma_{22}\\ \sigma_{33}\\ \sigma_{23}\\ \sigma_{31}\\ \sigma_{12}\end{bmatrix} = \begin{bmatrix} C_{11} & C_{12} & C_{13} & 0 & 0 & 0\\ C_{21} & C_{22} & C_{23} & 0 & 0 & 0\\ C_{31} & C_{32} & C_{33} & 0 & 0 & 0\\ 0 & 0 & 0 & C_{44} & 0 & 0\\ 0 & 0 & 0 & 0 & C_{55} & 0\\ 0 & 0 & 0 & 0 & 0 & C_{66}\end{bmatrix} \times \begin{bmatrix}\varepsilon^{d}_{11} + \frac{1}{3}\varepsilon_{vol}\\ \varepsilon^{d}_{22} + \frac{1}{3}\varepsilon_{vol}\\ \varepsilon^{d}_{33} + \frac{1}{3}\varepsilon_{vol}\\ \varepsilon_{23}\\ \varepsilon_{31}\\ \varepsilon_{12}\end{bmatrix}. \tag{5}$$

If the above relations are expanded, and the deviatoric and volumetric terms grouped separately, the following expressions for the direct stresses are

$$\sigma_{11} = \tfrac{1}{3}(C_{11} + C_{12} + C_{13})\varepsilon_{vol} + C_{11}\varepsilon^{d}_{11} + C_{12}\varepsilon^{d}_{22} + C_{13}\varepsilon^{d}_{33}, \tag{6a}$$

$$\sigma_{22} = \tfrac{1}{3}(C_{21} + C_{22} + C_{23})\varepsilon_{vol} + C_{21}\varepsilon^{d}_{11} + C_{22}\varepsilon^{d}_{22} + C_{23}\varepsilon^{d}_{33}, \tag{6b}$$

$$\sigma_{33} = \tfrac{1}{3}(C_{31} + C_{32} + C_{33})\varepsilon_{vol} + C_{31}\varepsilon^{d}_{11} + C_{32}\varepsilon^{d}_{22} + C_{33}\varepsilon^{d}_{33}. \tag{6c}$$

To find the equivalent pressure, we first define the pressure as a third of the trace of the stresses:

$$P = -\tfrac{1}{3}(\sigma_{11} + \sigma_{22} + \sigma_{33}). \tag{7}$$

Substituting (6) into (7) results in an expression for the pressure of the form

$$P = -\frac{1}{9}[C_{11} + C_{22} + C_{33} + 2(C_{12} + C_{23} + C_{31})]\varepsilon_{vol}$$

$$-\frac{1}{3}[C_{11}+C_{12}+C_{13}]\varepsilon_{11}^{d}$$
$$-\frac{1}{3}[C_{21}+C_{22}+C_{23}]\varepsilon_{22}^{d}$$
$$-\frac{1}{3}[C_{31}+C_{32}+C_{33}]\varepsilon_{33}^{d} \quad (8)$$

from which the contributions to the pressure from volumetric and deviatoric components of strain can clearly be identified.

For an isotropic material the first term on the right-hand side is equivalent to a linear EOS, whilst the remaining deviatoric strain terms would be zero. Thus, for an orthotropic material, the first term can be replaced with the Mie–Gruneisen EOS and the remaining terms act as a correction due to deviatoric strains:

$$P = P_r(\varepsilon_{vol}) + \frac{\Gamma(v)}{v}[e_r - e_r(\varepsilon_{vol})]$$
$$-\frac{1}{3}[C_{11}+C_{12}+C_{13}]\varepsilon_{11}^{d}$$
$$-\frac{1}{3}[C_{21}+C_{22}+C_{23}]\varepsilon_{22}^{d}$$
$$-\frac{1}{3}[C_{31}+C_{32}+C_{33}]\varepsilon_{33}^{d}. \quad (9)$$

The parameters $P_r(\varepsilon_{vol})$ and $e_r(\varepsilon_{vol})$, respectively, define the material pressure volume and energy–volume relationship along a reference curve known as the shock Hugoniot. The Gruneisen gamma, $\Gamma(v)$, allows extrapolation to material states off the reference curve and is a thermodynamic property of the material.

3.2. Tensile failure and reduction in shear stiffness

Tensile failure initiation can be based on any combination of the material stress and/or strain in the orthotropic principal material directions. After failure initiation, the failed material stiffness and strength properties are modified depending on the failure initiation modes. For example, in a laminate with material 11-direction through its thickness, the stress in the 11-direction is *instantaneously* set to zero if delamination occurs from excessive through thickness stresses (or strains) or from excessive shear stresses (or strains) in the matrix material. Subsequently, if the strain in the material along the 11-direction is tensile, the material stiffness matrix is modified as

$$\begin{bmatrix}\sigma_{11}\\ \sigma_{22}\\ \sigma_{33}\\ \sigma_{23}\\ \sigma_{31}\\ \sigma_{12}\end{bmatrix} = \begin{bmatrix}0 & 0 & 0 & 0 & 0 & 0\\ 0 & C_{22} & C_{23} & 0 & 0 & 0\\ 0 & C_{32} & C_{33} & 0 & 0 & 0\\ 0 & 0 & 0 & \alpha C_{44} & 0 & 0\\ 0 & 0 & 0 & 0 & \alpha C_{55} & 0\\ 0 & 0 & 0 & 0 & 0 & \alpha C_{66}\end{bmatrix} \times \begin{bmatrix}\varepsilon_{11}^{d}+\frac{1}{3}\varepsilon_{vol}\\ \varepsilon_{22}^{d}+\frac{1}{3}\varepsilon_{vol}\\ \varepsilon_{33}^{d}+\frac{1}{3}\varepsilon_{vol}\\ \varepsilon_{23}\\ \varepsilon_{31}\\ \varepsilon_{12}\end{bmatrix}. \quad (10)$$

Delamination will also result in a reduction in shear stiffness of the composite material. The parameter α, which accounts for this effect ranges between 0.0 and 1.0. In-plane failure is assumed to result from excessive stresses and/or strains in the 22- or 33-directions. If failure is initiated from these two modes, the stress in the failed direction is instantaneously set to zero. Subsequently, if the material strain in the 22- or 33-directions is tensile, the material stiffness matrix is modified. For example, for 22-direction failure the post-failure stiffness matrix becomes

$$\begin{bmatrix}\sigma_{11}\\ \sigma_{22}\\ \sigma_{33}\\ \sigma_{23}\\ \sigma_{31}\\ \sigma_{12}\end{bmatrix} = \begin{bmatrix}C_{11} & 0 & C_{13} & 0 & 0 & 0\\ 0 & 0 & 0 & 0 & 0 & 0\\ C_{31} & 0 & C_{33} & 0 & 0 & 0\\ 0 & 0 & 0 & \alpha C_{44} & 0 & 0\\ 0 & 0 & 0 & 0 & \alpha C_{55} & 0\\ 0 & 0 & 0 & 0 & 0 & \alpha C_{66}\end{bmatrix} \times \begin{bmatrix}\varepsilon_{11}^{d}+\frac{1}{3}\varepsilon_{vol}\\ \varepsilon_{22}^{d}+\frac{1}{3}\varepsilon_{vol}\\ \varepsilon_{33}^{d}+\frac{1}{3}\varepsilon_{vol}\\ \varepsilon_{23}\\ \varepsilon_{31}\\ \varepsilon_{12}\end{bmatrix}. \quad (11)$$

Finally, the combined effect of failure in all three material directions results in a material that can only sustain hydrostatic pressure. Fractional residual shear stiffness is maintained and determined based on the parameter α and the maximum post-failure shear stress can also be limited based on a predefined value.

3.3. Melting, vaporization and decomposition

The melting, vaporization and decomposition of KEVLAR®/Epoxy has been observed in flyer plate impact tests at velocities of around 1000 m/s [8]. In the model it is assumed that the melting of the binder material, better known as the matrix material, will have a very similar effect to delamination occurring in tensile strain fields. If the

temperature of the composite material exceeds the matrix's melting temperature, delamination is assumed to occur. In the modeling of the decomposition of KEVLAR®/Epoxy, the decomposition temperature for the fiber can also be specified. When the KEVLAR®/Epoxy is subjected to compression at this temperature, the decomposed material will assume the intact material properties. However, when the composite material is subjected to bulk tension at this temperature, pressure, deviatoric and tensile stresses in the material will assume to have null values.

4. Hydrocode simulation of spherical projectile impact on a KEVLAR® helmet

This is an initial study exploring the prospect of combining ballistic tests and hydrocode simulations to determine if a KEVLAR® helmet is able to conform to ballistic test standards. The modeling of the KEVLAR® helmet begins by measuring the geometrical coordinates of the helmet to construct its surfaces, and they are obtained using a CMM or coordinate measuring machine. Fig. 3 shows the measuring process using the CMM. A hexahedral mesh was then generated from these surfaces using TrueGrid® [12] and imported into AUTODYN-3D®. The contact, sliding and separation between the projectile and the helmet are defined using the *gap* interaction logic. With the *gap* interaction logic, each surface segment is surrounded by a contact detection zone; the radius of this detection zone is called the gap size. Any nodes entering the detection zone of a surface segment are repelled by a force proportional to the depth of penetration of the node into the detection zone. The gap size used in this simulation is 0.1111 mm. The material model outlined in Section 3 is used to represent the response of the KEVLAR® helmet to ballistic impact, and the constants for the material model are listed Table 1. These constants are for KEVLAR® 129 [8]. To fully characterize the KEVLAR® 29 material would require an extensive series of experimental tests [8]. Hence, in this simulation we use the material constants for KEVLAR® 129 to predict the ballistic resistance of a KEVLAR® 29 helmet. We hypothesize that the difference in material properties will not adversely affect the prediction. This hypothesis is first tested by validating the hydrocode simulation against the ballistic test outlined in Section 2. To reproduce the ballistic test, a spherical projectile is assigned an initial velocity so that it strikes the back of the helmet at 205 m/s. Data for the stainless steel spherical projectile are obtained from the standard AUTODYN material library.

The simulation is consistent with the experiment. Fig. 4 compares the images captured using high-speed photography with those from numerical simulation at 0.06 ms. Fig. 5 shows the post-test photos of the helmet and images from the hydrocode simulation. Both the experiment and simulation indicate that the projectile did not penetrate the

Table 1
Input for the material model for the KEVLAR® helmet [8] in AUTODYN-3D®

Parameter	Value
Ref. density (g/cm^3)	1.65
EOS	Ortho
Young modulus 11 (kPa)	1.7989e+07
Young modulus 22 (kPa)	1.7989e+07
Young modulus 33 (kPa)	1.9480e+06
Poisson ratio 12	0.0800
Poisson ratio 23	0.6980
Poisson ratio 31	0.0756
Shear modulus 12 (kPa)	1.85701e+06
Shear modulus 23 (kPa)	2.23500e+05
Shear modulus 31 (kPa)	2.23500e+05
Strength	Elastic
Shear modulus (kPa)	1.85701e+06
Failure	Material Stress/ Strain
Tensile failure strain 11	0.06
Tensile failure strain 22	0.06
Tensile failure strain 33	0.02
Post-failure option	Orthotropic
Residual shear stiffness fraction	0.20
Failed in 11, failure mode	11 only
Failed in 22, failure mode	22 only
Failed in 33, failure mode	33 only
Failed in 12, failure mode	12 & 33 only
Failed in 23, failure mode	23 & 33 only
Failed in 31, failure mode	31 & 33 only
—	—

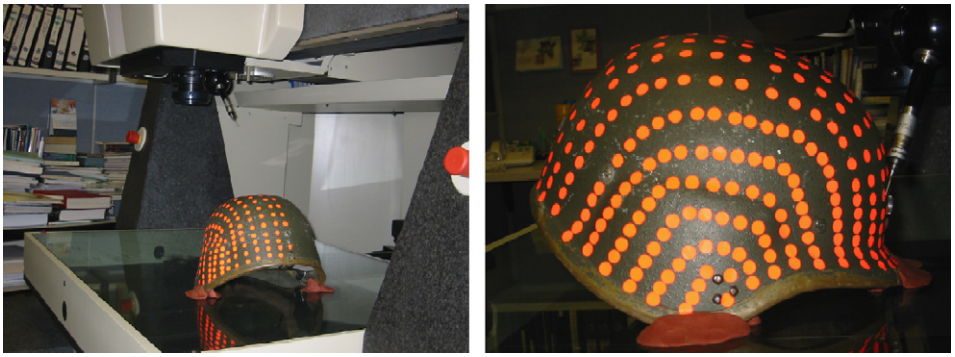

Fig. 3. "Picking-up" the coordinates to generate the CAD surface of the KEVLAR® helmet using a CMM.

helmet. However, the helmet did experience slight damage on the impact region. The post-test photograph in Fig. 6 indicates the helmet was indented and some layers of paint were ejected from the impact surface. The indentation, which was also observed in the hydrocode simulation, has the highest effective strain. Table 2 compares the diameter of the impression and the depth of penetration with those obtained from the experiment. The diameter and depth of penetration from the experiment should only be seen as indicative as it is often difficult to make precise measurements, moreover these dimensions could also be subjected to experimental scatter. Nonetheless overall results from the hydrocode simulation are consistent with observations from the experiment.

5. Predicting the ballistic limit of a KEVLAR® laminate using AUTODYN-3D®

Hydrocode simulations were performed to determine the V_{50} ballistic limit of a 9.5 mm thick KEVLAR® 29 laminate with 15–18% phenol formaldehyde and polyvinyl butyral resins. The purpose of this simulation is to further verify the composite material model and to determine whether the curvature of the helmet has an effect on the V_{50} ballistic limit. The projectile used in the simulation is a 1.1 g FSP based on STANAG 2920. Fig. 7 shows the mesh for the FSP created using TrueGrid®. For this numerical simulation, the projectile and the laminate are modeled using a Lagrangian mesh and symmetrical boundary conditions are imposed on the $X = 0$ and $Y = 0$ planes to reduce the size of the computational domain. The computational domain of the laminate is defined in the I–J–K space with IMAX = 43, JMAX = 29 and KMAX = 11, and it is constrained at I = 43 and J = 29 planes in the z-direction. Fig. 8 presents the model for the

Table 2
Diameter of impression and depth of penetration from experiment and AUTODYN-3D® simulation

Results	Diameter of impression (mm)	Depth of penetration (mm)
AUTODYN-3D® simulation	12.2	0.7
Experiment	12	0.5

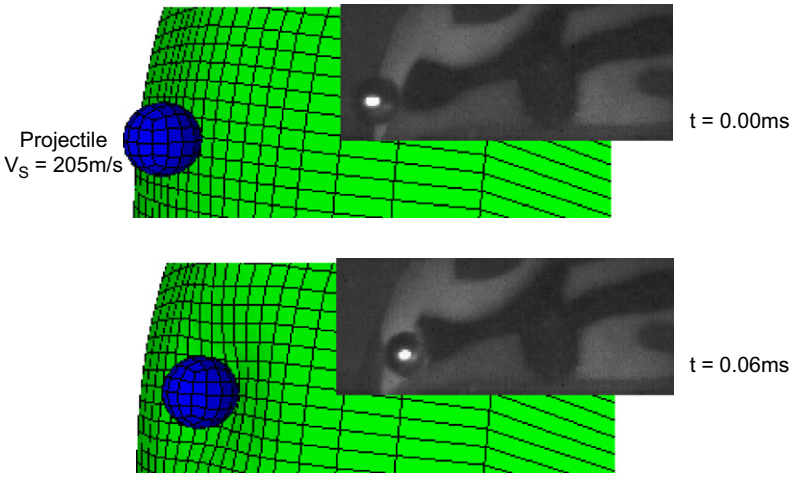

Fig. 4. Images from high-speed photography and hydrocode simulation on the ballistic impact of a KEVLAR® helmet.

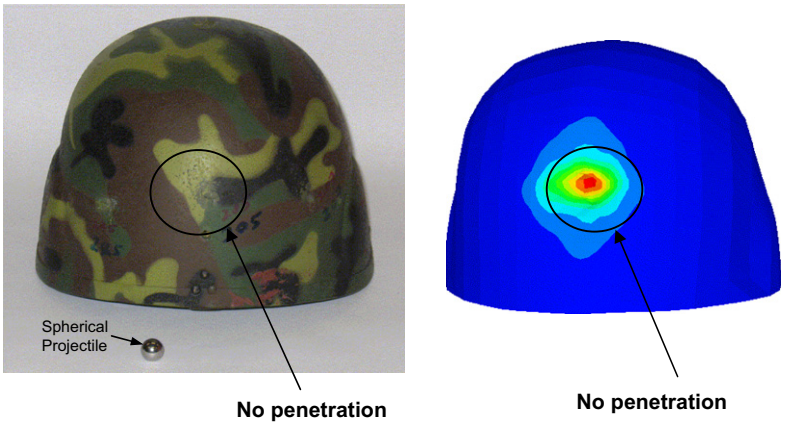

Fig. 5. No penetration is observed in both experiment and hydrocode simulation.

FSP and the KEVLAR® 29 laminate before impact. A uniform cell size of 0.5461 mm in both *I* and *J*-directions is defined for the impact region, which is 9.2837 × 9.2837 mm. The gap size used in this simulation is 0.0096 mm. The FSP, machined from AISI 4340 steel, is assumed to have a strain-hardening, strain-rate and temperature dependent yield function with a Mie–Gruneisen EOS. The constants for the yield function and EOS are obtained from the standard AUTODYN material library.

V_{50} ballistic limit is defined as a striking velocity for which there exist a 50% probability of perforation of the barrier or some protective device [13]. In the simplest approach, a V_{50} is determined by averaging six projectile-striking velocities that include three lowest velocities that resulted in complete penetration and the three highest velocities that resulted in a partial penetration. In this simulation the KEVLAR® 29 laminate is subjected to two striking velocities, 590 and 630 m/s, to determine the V_{50} ballistic limit. This ballistic limit is determined to be at 610 m/s. In Fig. 9 the result shows that a FSP striking at 610 m/s is able to defeat a 9.5 mm thick KEVLAR® laminate. The V_{50} from the simulation are in close agreement with that from the ballistic test reported in [14]. Table 4 summarizes both the simulation and the experimental results. The simulation also indicates that the assumption of using the material constants of KEVLAR® 129 has no adverse affect on the ballistic limit prediction of the KEVLAR® 29 laminate. Clegg and co-workers [9] used material constants for KEVLAR® 129 to predict the backplane velocity at two points of a KEVLAR® 29

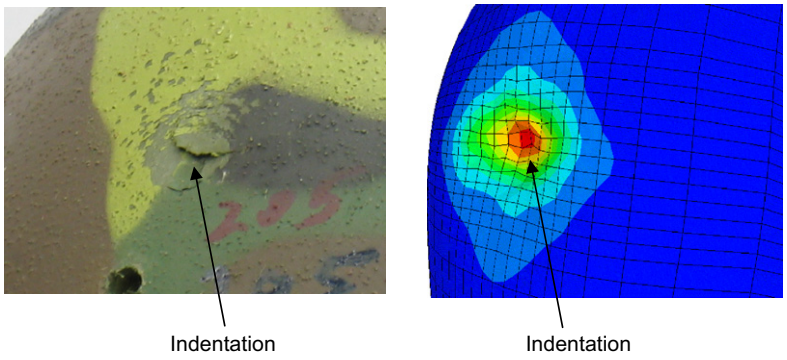

Fig. 6. Indentation is observed in both experiment and hydrocode simulation.

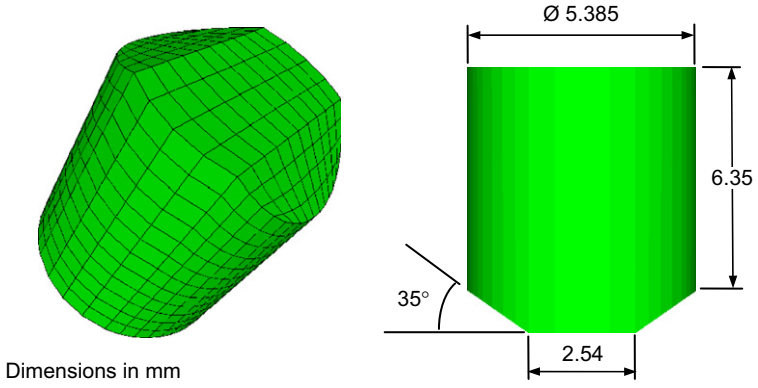

Fig. 7. The geometry and the mesh for the FSP.

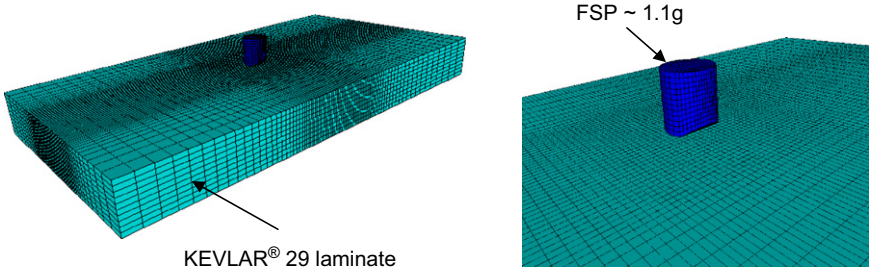

Fig. 8. The initial meshes for the FSP and the KEVLAR® 29 laminate.

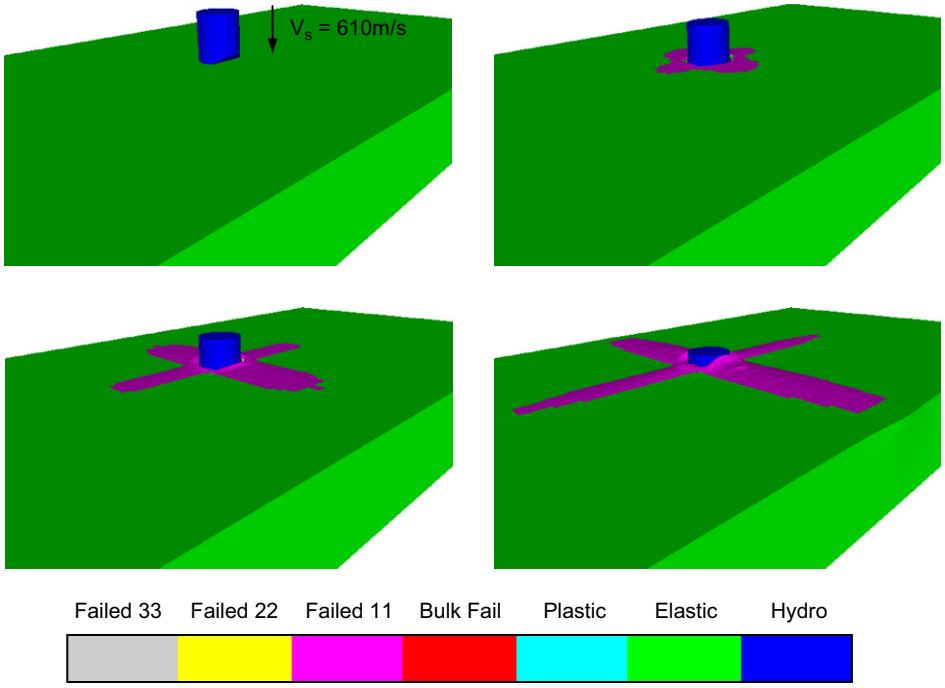

Fig. 9. Failure plots at $t = 0$, 2.5, 5.0 and 10 μs.

laminate (i.e. 19 layers) with epoxy matrix demonstrated that the simulated projectile velocity–time history compared reasonably well with the results from experiment.

6. Predicting the ballistic limit of a KEVLAR® laminate using analytical equation

Walker developed an analytical equation to predict the ballistic limit curve of a fabric/resin panel from the ballistic limit curve of the dry fabric [15]. The ballistic limit of the dry fabric, obtained through the strain equation from static deflection, is given by

$$V_{\mathrm{bl}}(X,0) = \frac{9}{2}(1+\beta X)c_{\mathrm{f}}\varepsilon_{\mathrm{f}}\left\{\left(\frac{R_{\mathrm{bl}}}{R_{\mathrm{p}}}\right)^{2/3} - 2\left(\frac{R_{\mathrm{bl}}}{R_{\mathrm{p}}}\right)^{1/3} + 3\right\}, \tag{12}$$

where $R_{\mathrm{bl}}/R_{\mathrm{p}}$ and X are defined as follows

$$\frac{R_{\mathrm{bl}}}{R_{\mathrm{p}}} = \sqrt{\frac{9\pi}{8}\left(\frac{1}{X}+\beta\right)}, \tag{13}$$

$$X = \frac{\tilde{\rho}A_{\mathrm{p}}}{m_{\mathrm{p}}}, \tag{14}$$

The ballistic limit for a fabric/resin panel is a function of the ballistic limit of the dry fabric:

$$V_{\mathrm{bl}}(X,r) = \sqrt{1-r+r(\beta X)^3}\,V_{\mathrm{bl}}(X,0), \tag{15}$$

where r is the mass fraction of resin in the system (i.e. $r = 0$ for dry fabric and $r = 1$ for pure resin system). Table 3 provides the material and physical properties of the KEVLAR® and the FSP. With these properties, the second row of Table 4 tabulates the ballistic limit calculated using Eq. (15). Table 4 compares the V_{50} from hydrocode simulation, analytical equation [15] and ballistic test [14].

Table 3
Material and physical properties of the FSP and the KEVLAR® laminate

$\tilde{\rho}$ (g/cm^2)	A_{p} (cm^2)	m_{p} (g)	β	r
0.9025	0.22775	1.1	2.56	0.18

Table 4
V_{50} of a 9.5 mm thick KEVLAR® laminate

Results	V_{50} (m/s)
AUTODYN-3D® simulation	610
Analytical equation [15]	575
Ballistic test [14]	600

7. Hydrocode simulation of FSP impact on a KEVLAR® helmet

Another hydrocode simulation was performed to determine if a KEVLAR® helmet could defeat a FSP, described in Fig. 7, striking at the top which is approximately 9.5 mm thick. The simulation is performed using AUTODYN-3D®. Fig. 10 illustrates the KEVLAR® helmet and the FSP before impact. In this numerical simulation, the rim of the KEVLAR® helmet is fixed along the x, y and z direction and the FSP is given an initial velocity of 610 m/s. The gap size used in this simulation is 0.009601 mm. The constants for the material model for the KEVLAR®

helmet are provided in Table 1. In this fragment impact simulation, the KEVLAR® helmet is expected to experience severe deformation when the fragment penetrates the laminate, thus calculation using the Lagrange solution technique will result in excessive cell distortion and tangling. To prevent the calculation from terminating prematurely due to cell distortion and tangling, an erosion logic based on an instantaneous geometric strain is assigned to the KEVLAR® helmet. The erosion logic, which is not a representation of the physical process, automatically removes the distorted cells when the instantaneous geometric strain of these cells exceeds a predefined setting and the compressive strength of a cell is lost when it is eroded. Thus, cells should only be eroded when they are severely distorted and its compressive strength is not likely to effect the calculation. In [11], the recommended value for erosion is in the range of 150–200%. For this simulation the erosion for the KEVLAR® helmet is set at 150% and the response of the laminate to impact is represented using the model outlined in Section 3. According to MIL-H-44099A, the manufacturers of PASGT Helmets complying with this specification have to ensure that the V_{50} ballistic limit for each helmet shall not be less than 610 m/s when tested according to the procedure specified. Based on this hydrocode simulation, the results presented in Fig. 11 confirm that the KEVLAR® helmet can provide protection against a FSP traveling at 610 m/s. This result infers that the V_{50} ballistic limit for the KEVLAR® helmet is higher than 610 m/s. Cunniff [16] presented the results of a regression analysis for the V_{50} of KEVLAR® 29 helmets. The V_{50} obtained from his analysis is 660 m/s. Hydrocode simulation of the KEVLAR helmet was also performed and the result is summarized in Table 5, which also

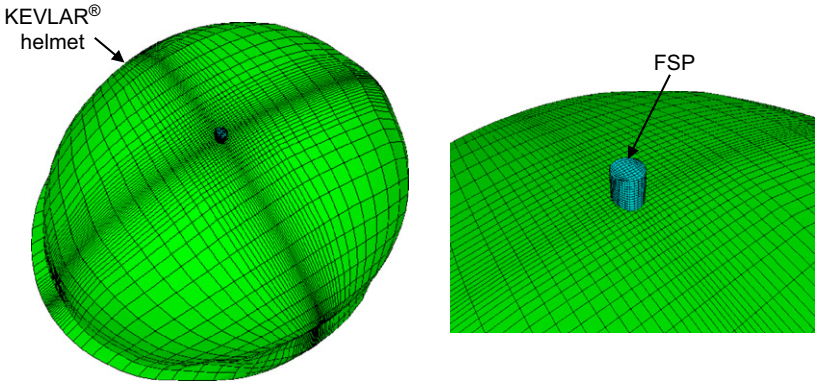

Fig. 10. The initial meshes for the KEVLAR® helmet with the FSP before impact.

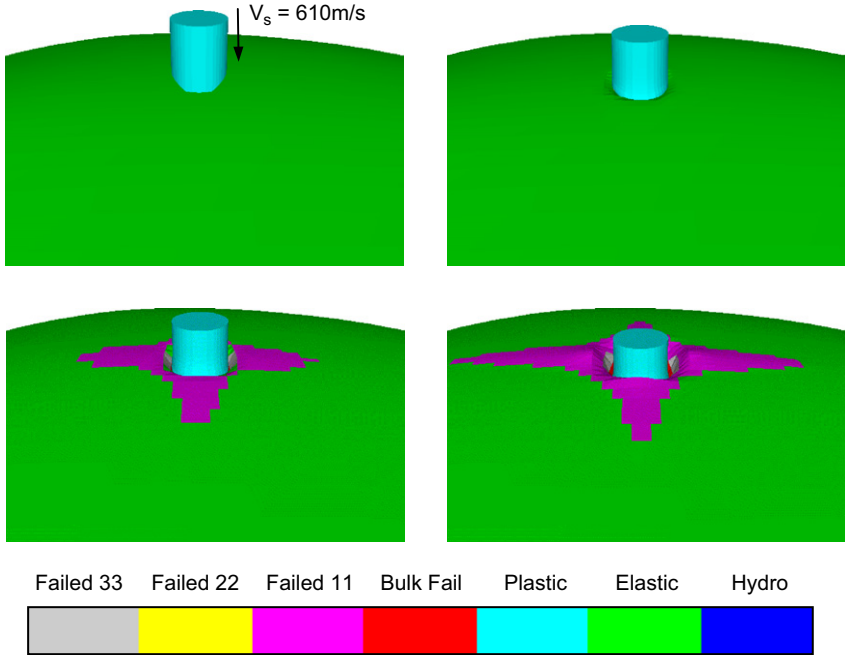

Fig. 11. Failure plots with FSP striking at the top at $t = 0$, 2.5, 5.0 and 10 μs.

compares this result with that obtained from Cunniff's regression analysis.

On impact at V_{50}, a compressive wave is generated. This wave propagates through the thickness of the helmet and is reflected as a tensile wave from its interior surface. This tensile wave could cause tensile failure in the matrix interface between plies of KEVLAR® fabric resulting in delamination. Fig. 12 plots the variation of the pressure wave with time at the interior surface of the helmet opposite the point of impact. The maximum pressure recorded is 8.0E + 05 kPa at approximately 3.5 μs after impact. The deformation of the helmet changes as the FSP penetrates through the helmet. The early stage of the penetration is dominated by compression, and displacement of the KEVLAR® material ahead of the projectile. The latter stage is characterized by stretching and shearing of the fibers adjacent to the projectile. Fig. 13 illustrates the stretching of the fibers. The inclined face of the FSP causes less shearing of the fibers, but stretches adjacent fibers till they suffer from tensile failure. This observation may suggest that the shape of the projectile could have an influence on the penetration process. The radial expansion of the deformed cone is shown in Fig. 14. The damage observed was in the form of a cone opening towards the interior of the helmet. This cone of delamination also opens towards the impact side for sufficiently thick targets [17]. The cone of delamination on the impact side is interpreted as a consequence of the compression of KEVLAR® material ahead of the FSP. This leads to radial pressure which causes an "upflow" of materials as seen in Fig. 13. Finally, comparing the results from Tables 4 and 5 seems to indicate that there is a slight difference in ballistic resistance for a KEVLAR® laminate and helmet. Although they have a thickness of 9.5 mm, the helmet offers a slightly higher ballistic resistance than the laminate.

Table 5
V_{50} of a KEVLAR® helmet

Results	V_{50} (m/s)
AUTODYN-3D® simulation	680
Cunniff [16]	660

8. Hydrocode simulation of 9 mm FMJ impact on a KEVLAR® helmet

A hydrocode simulation was also performed to determine if the KEVLAR® helmet is able to conform to NIJ-STD-0106.01 Type II, higher velocity 9 mm. The geometry of the 9 mm FMJ is provided in Fig. 15. The mesh for the bullet, also shown in Fig. 15, is created using TrueGrid®. The bullet consists of two parts: (1) a brass jacket and (2) a lead core. The shear response of the brass jacket and the lead core is modeled using the Johnson–Cook and the Steinberg–Guinan strength models, respectively. The response of these two materials under high pressure compression is described using the Mie–Gruneisen EOS. The constants for the material models and EOS can be found in [18,19]. In assessing the ballistic resistance of KEVLAR® helmet based on NIJ-STD-0106.01 Type II, higher velocity 9 mm, the FMJ is assigned an initial velocity of 358 m/s in the simulation.

8.1. Side impact

Fig. 16 presents the AUTODYN-3D® model for the KEVLAR® helmet for side impact. Fixed boundary conditions along the x, y and z directions are imposed onto the rim of the helmet. The gap size used in this simulation is 0.022 mm. The position of the 9 mm FMJ with respect to the KEVLAR® helmet prior to impact is illustrated in Fig. 16. Results from the simulation and ballistic test [20] shown in Fig. 17 demonstrate that the KEVLAR® helmet is able to stop and defeat a 9 mm FMJ striking at the side. The simulation also reveals that the

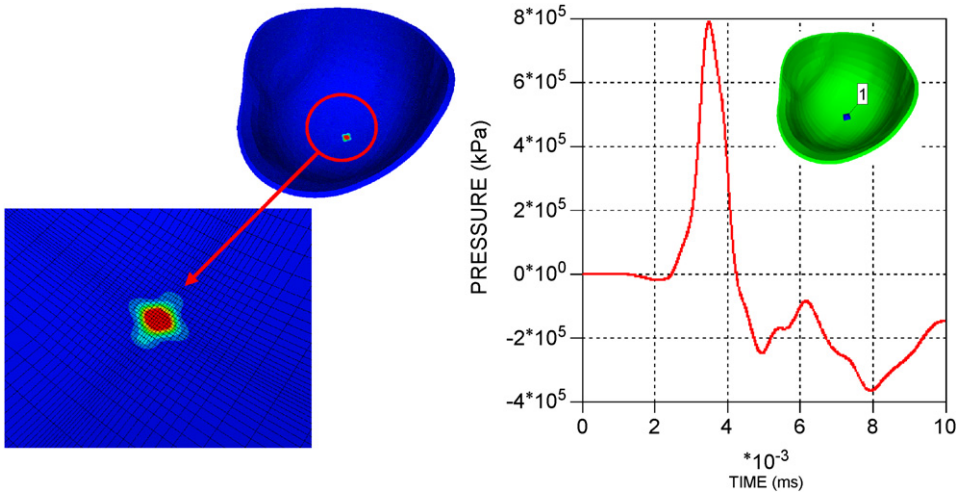

Fig. 12. Pressure in the helmet with FSP striking at the top at V_{50}.

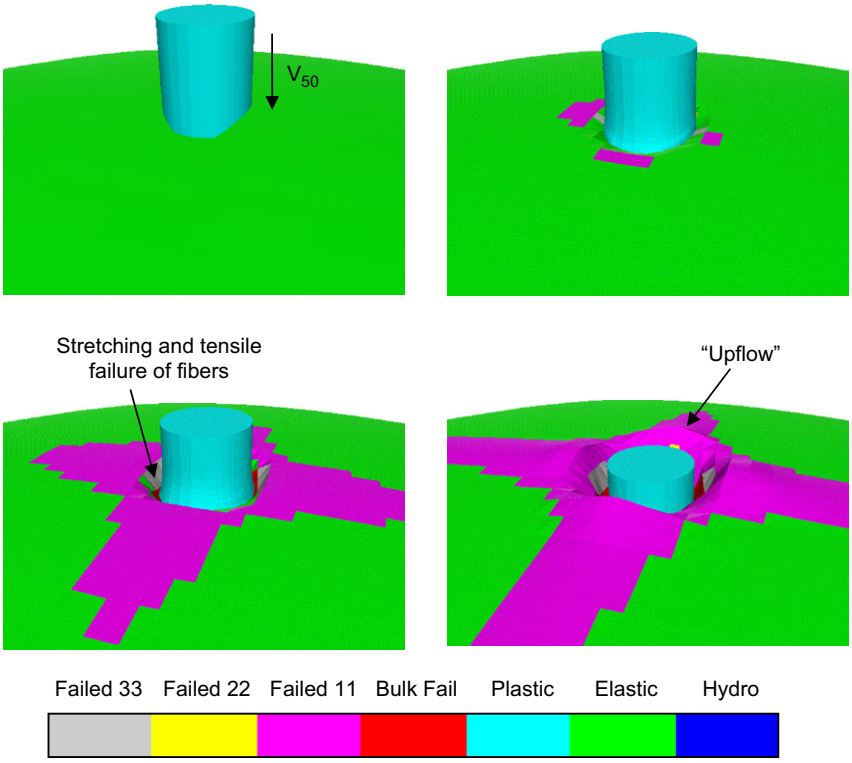

Fig. 13. Stretching and tensile failure of fibers at V_{50}.

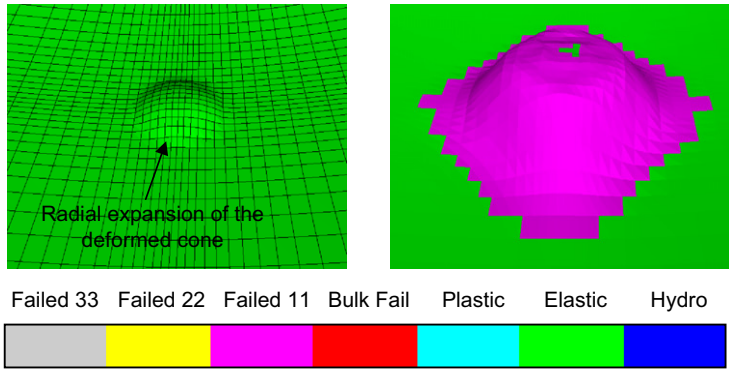

Fig. 14. Backface deformation of the helmet at V_{50}.

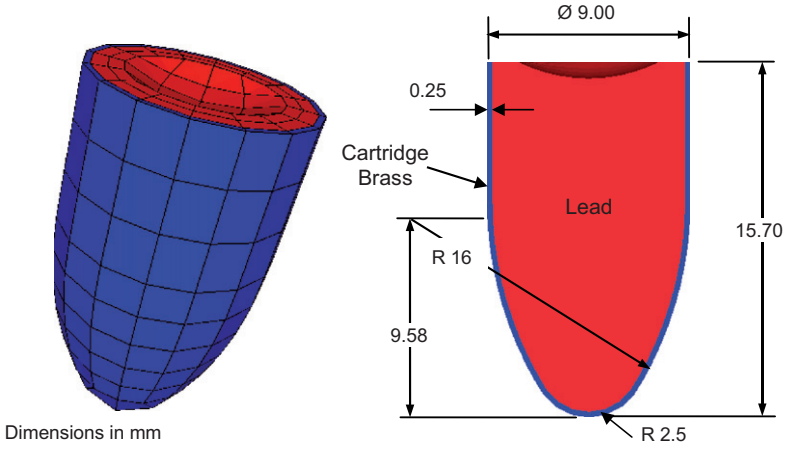

Fig. 15. The geometry and mesh for the 9 mm FMJ.

9 mm bullet deforms severely after impact—manifestation of the "mushrooming" at the tip of the bullet.

8.2. Top impact

A normal impact at the top of the helmet is also simulated. Similar to the model for side impact, the mesh for the helmet is also created using TrueGrid® and then imported into AUTODYN-3D®. Likewise, the rim of the helmet is fixed along the x, y and z directions. Fig. 18 presents the AUTODYN-3D® model for 9 mm FMJ in relation to the KEVLAR® helmet. Results from the simulation, in Fig. 19, indicate the KEVLAR® helmet is able to stop and defeat a 9 mm FMJ striking at the top. Similar to the case for side impact, the 9 mm bullet deformed after impact with "mushrooming" at the nose of the projectile.

9. Conclusions

The 21st century military helmets have to be designed with lighter fiber materials, and yet are expected to provide increased ballistic protection from fragments and bullets. To ensure that these improved helmets are able to provide adequate protection, they are subjected to a series of ballistic tests based on the requirements specified in test standards from government agencies. This process can be expensive when exploring design variations during the development of the next generation of ballistic helmets. Hydrocode simulations can alleviate the expense incurred during the development of these new helmets. Through hydrocode simulations, helmet designers can cost-effectively explore and assess the ballistic resistance of prototype helmets which are designed using cheaper, lighter and stronger fiber materials.

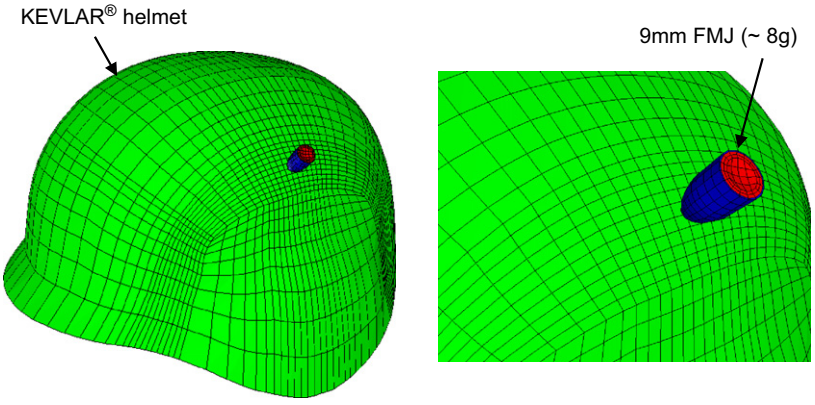

Fig. 16. The initial meshes for the KEVLAR® helmet with the 9 mm FMJ before impact.

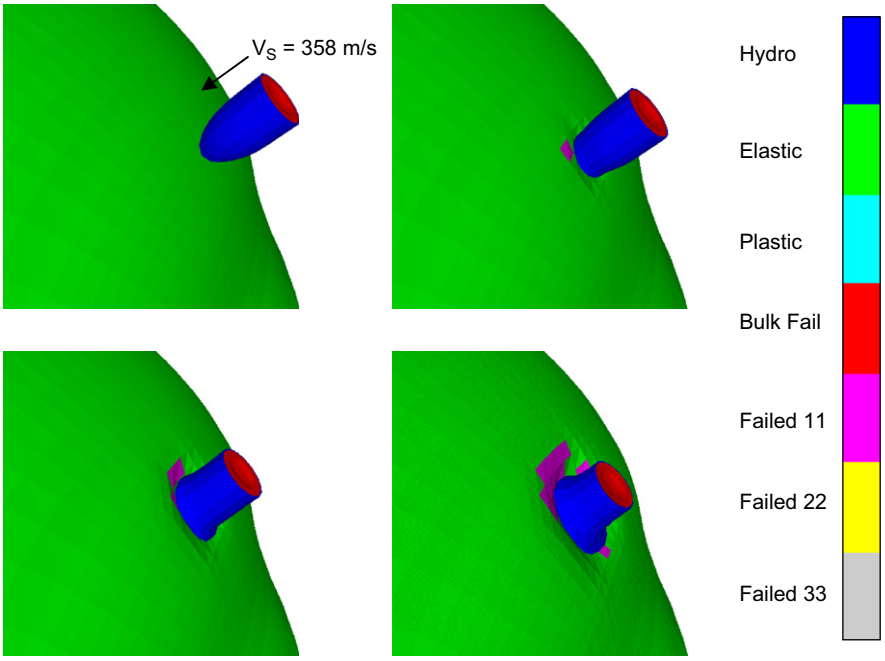

Fig. 17. Failure plots with the 9 mm FMJ striking at the side at $t = 0$, 0.01, 0.02 and 0.03 ms.

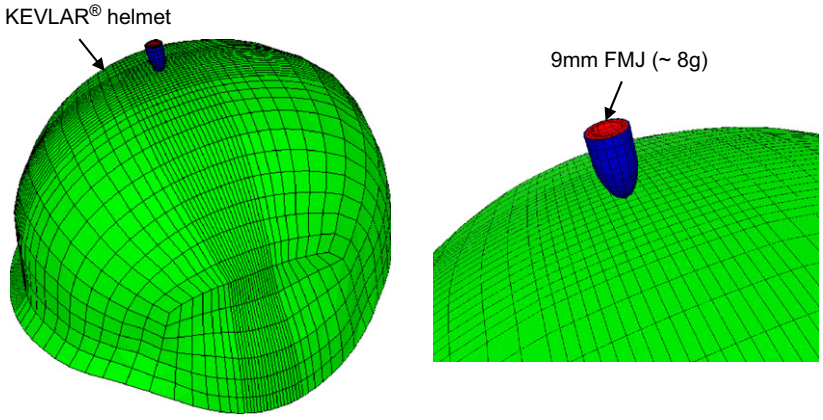

Fig. 18. The initial meshes for the KEVLAR® helmet with the 9 mm FMJ before impact.

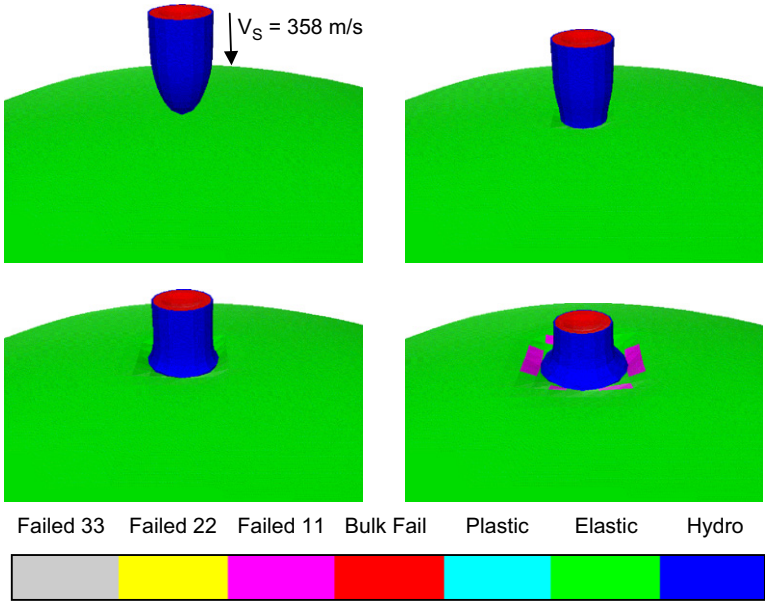

Fig. 19. Failure plots with the 9 mm FMJ striking at the top at $t = 0$, 0.01, 0.02 and 0.03 ms.

In this paper we presented the results from a ballistic impact test of a KEVLAR® helmet and also demonstrated the application of hydrocode simulations in assessing its ballistic resistance. In the ballistic impact tests, steel spherical projectiles of mass 11.9 g struck the back of a helmet at 205 m/s. High-speed images from the ballistic impact tests revealed that the KEVLAR® helmet was able to defeat the steel spherical projectile. Three hydrocode simulations were also performed to assess the ballistic resistance of the KEVLAR® helmet. These three simulations were: (1) hydrocode simulation of fragment impact on a KEVLAR® laminate. (2) Hydrocode simulation of fragment impact on a KEVLAR® helmet. (3) Hydrocode simulation of 9 mm FMJ impact on a KEVLAR® helmet. In these simulations, the KEVLAR® material was described using a material model that coupled the anisotropic constitutive behavior of KEVLAR® with its non-linear (shock) EOS. In (1), the V_{50} ballistic limit of a 9.5 mm thick KEVLAR® laminate against a FSP was determined using hydrocode simulations to be 610 m/s. The prediction was in agreement with experimental test result of 600 m/s and analytical result of 575 m/s. In (2), hydrocode simulations were also used to determine the V_{50} of the KEVLAR® helmet against a FSP. The simulation indicated the KEVLAR® helmet can provide protection against a FSP traveling at up to 610 m/s. Furthermore the results from (1) and (2) show that the KEVLAR® helmet and laminate has slight differences in their ballistic resistance. In (3), hydrocode simulations were used to determine if the KEVLAR® helmet was able to defeat a 9 mm FMJ with an impact velocity of 358 m/s. Simulations and ballistic tests [19] confirmed that the KEVLAR® helmet was able to stop the projectile. Furthermore hydrocode simulations for both side and top impacts showed that the 9 mm bullet deformed after impact, indicating that the helmet was capable of stopping the bullet coming from either direction. Finally, by comparing these aforementioned simulations with ballistic

test data, it is concluded that the model presented in Table 1 is adequate in simulating the two ballistic test standards for KEVLAR® 29 helmets.

Acknowledgments

The authors would like to thank C. W. Low and T. L. Goh of the Impact Mechanics Laboratory, National University of Singapore for their help in conducting the experiment.

References

[1] Carey ME, Herz M, Corner B, McEntrie J, Malabarba D, Paquette S, et al. Ballistic helmet and aspect of their design. Neurosurgery 2000;47(3):678–89.
[2] Laible RC, editor. Ballistic materials and penetration mechanics. Amsterdam: Elsevier; 1980.
[3] Reynosa MA. The Personnel Armor System Ground Troops (PASGT) helmet. Schiffer Military History; 1999.
[4] Technical Guide for KEVLAR® Aramid Fiber, H-77848, DuPont, 2000.
[5] Bolduc M, Nandall D. Evaluation of the transient deformation of military helmets. In: Proceedings of the 14th international symposium on ballistics, Que., Canada; 1993.
[6] McIntosh GWJ, Blais J. Performance evaluation of novel helmets. DRDC-Valcartier TN 2003-250. Defence Research & Development Canada, Valcartier; 2004.
[7] Hayhurst CJ, Hiermaier SJ, Clegg RA, Reidel W, Lambert M. Development of material models for Nextel and Kevlar-Epoxy for high pressures and strain rates. Int J Impact Eng 1999;23:365–76.
[8] Hiermaier SJ, Riedel W, Clegg RA, Hayhurst CJ. Advanced material model for hypervelocity impact simulations. ESA Contract No. 12400/97/NL/PA(SC) Final Report, July 1999.
[9] Clegg RA, Hayhurst CJ, Leahy J, Deutekom M. Application of a coupled anisotropic material model to high velocity impact response on composite textile armor. In: Proceedings of the 18th international symposium on ballistics, San Antonio, TX, USA; 1999. p. 791–8.
[10] Anderson CE, Cox PA, Johnson GR, Maudlin PJ. A constitutive formulation for anisotropic materials suitable for wave propagation computer programs—II. Comput. Mech. 1994;15:201–23.
[11] AUTODYN. Theory manual, revision 4.0, Century Dynamics Inc., 1998.
[12] TrueGrid, Livermore, CA, USA. XYZ Scientific Applications, Inc, 2000.
[13] Zukas JA, Nicholas T, Swift HF, Greszczuk LB, Curran DB. Impact dynamics. New York: Kreiger Publishing Company; 1992.
[14] van Hoof J, Worswick MJ, Straznicky PV, Bolduc M. Effects of post-failure modeling on the response of ballistically impacted composites. In: Proceedings of the 12th international conference on composite materials, Paris, France; 1999.
[15] Walker JD. Ballistic limit of fabrics with resin. In: Proceedings of the 19th international symposium on ballistics, Interlaken, Switzerland, 2001. p. 1409–14.
[16] Cunniff PM. Decoupled response of textile body armor. In: Proceedings of the 18th international symposium on ballistics, San Antonio, TX, USA, 1999. p. 814–21.
[17] Gellert EP, Cimpoeru RL, Woodward WL. A study of the effect of target thickness on the ballistic perforation of glass-fiber-reinforced plastic composites. Int J Impact Eng 2000;24:445–56.
[18] Johnson GR, Cook WH. A constitutive model and data for metals subjected to large strains, high strain rates and high temperatures. In: Proceedings of the seventh international symposium on ballistics, Hague, Netherlands, 1983.
[19] Steinberg DJ. Equation of state and strength properties of selected materials. UCRL-MA-106439. Livermore, CA: Lawrence Livermore National Laboratory; 1991.
[20] 〈http://www.bulletproofme.com/PHOTO%20pages/Kevlar_Helmets_PHOTOS.shtml〉.